Catalytic ignition of CO over CuCeZr based catalysts: New insights into the support effects and reaction pathways

Running Kang[a,b,c], Zirui Zhang[a], Feng Bin[a,b*], Xiaolin Wei[a,b], Yongdan Li[c], Guoxing Chen[d*], Xin Tu[e*]

[a] *State Key Laboratory of High-Temperature Gas Dynamics, Institute of Mechanics, Chinese Academy of Sciences, Beijing 100190, China*

[b] *School of Engineering Science, University of Chinese Academy of Sciences, Beijing 100049, China*

[c] *Department of Chemical and Metallurgical Engineering, School of Chemical Engineering, Aalto University, Kemistintie 1, Espoo, P.O. Box 16100, FI-00076, Finland*

[d] *Fraunhofer Research Institution for Materials Recycling and Resource Strategies IWKS, Brentanostraße 2a, 63755 Alzenau, Germany*

[e] *Department of Electrical Engineering and Electronics, University of Liverpool, Liverpool L69 3GJ, United Kingdom*

[*] Corresponding authors

binfeng@imech.ac.cn (F. Bin); guoxing.chen@iwks.fraunhofer.de (G. Chen); xin.tu@liverpool.ac.uk (X. Tu)

Abstract: Self-sustained catalytic combustion is a promising strategy to remove CO from the off-gas produced during steelmaking, where the potential catalysts are bulk copper-cerium-zirconium mixed oxides or those supported on TiO_2 or ZSM-5 substrates. In this study, the effects of the catalyst support on the CO catalytic ignition performance and reaction pathways were investigated by FTIR coupled with a novel in-situ cell, together with the state-of-the-art characterization techniques. The Infrared (IR) transmission cell equipped with a magnetically driven system, could effectively prevent overlaps between active intermediate peaks (Cu^+-CO and $Cu^+(CO)_2$) and gaseous CO peaks. The Cu^+ cations located at the phase interface are the main active sites. The Cu and Ce interactions lead to the formation of solid solutions of $CuCe_{0.75}Zr_{0.25}O_\delta$ (CuCeZr). The monocarbonyls [Cu^+-CO] are the dominant species during CO oxidation, and the vacancies in the solid solutions are occupied by oxygen, accelerating the oxygen cycle. The TiO_2 or ZSM-5 supports promote copper dispersion over $CuCe_{0.75}Zr_{0.25}O_\delta/TiO_2$ (CuCeZr/T) and $CuCe_{0.75}Zr_{0.25}O_\delta$/ZSM-5 (CuCeZr/Z) catalysts, which can be attributed to their high surface areas (168.2 and 346.3 m^2/g, respectively), while the Cu-Ce interactions are less relevant. Hence, CO oxidation mainly occurs at the phase interface between copper oxide and TiO_2/ZSM-5. Dicarbonyls [$Cu^+(CO)_2$] are the main intermediates for the CuCeZr/T and CuCeZr/Z catalysts, and the Cu^{2+} species are reduced to form dicarbonyls that also take part in the oxidation process. Although a well copper dispersion enhances the activity of individual copper sites on the CuCeZr/T and CuCeZr/Z catalysts, considering the redshift of the carbonyl bands and the increase in CO adsorption, the close

interactions and high contents of Cu and Ce favor the local accumulation of heat and mass transfer over bulk CuCeZr, leading to the ignition of CO at low temperatures.

Keywords: Carbon monoxide; Self-sustained catalytic combustion; Support effect; Copper-cerium-zirconium mixed oxide; Magnetically driven IR cell

1. Introduction

Carbon monoxide (CO), a colorless and odorless toxic gas with increased concentration in atmosphere can induce major threats to human being such as tissue hypoxia and even suffocate people to death. As a key heterogeneous process, the catalytic oxidation of CO is therefore essential not only for a practical point of view such as the purification of industrial off-gases and automotive exhaust gases, gas masks and gas sensors, CO_2 lasers and catalytic filters for indoor air cleaning, but also as a model reaction to study the reaction mechanism and structure-reactivity correlation of catalysts. Although the $CO \rightarrow CO_2$ reaction is exothermic ($CO + 1/2\ O_2 \rightarrow CO_2$, $\triangle H = -283$ kJ/mol, or 12.64 MJ/Nm^3), the generation rate of reaction heat is less than that of released heat since the CO concentration in the above applications is usually less than 1 vol.%. Therefore, the existing studies are mainly limited to the intrinsic reaction kinetic stage with low reaction rate, where the temperature of catalyst bed close to the controlled temperature.

Chinese crude steel output in 2020 exceeded 1.03 billion tons, accounting for 56.5% of total world output. The basic oxygen furnace (BOF), accounting for over 70% of global steel production, is a subprocess in steelmaking where hot metal is converted into molten steel by reducing the carbon content [1]. Evidently, the off-gas from converter gas is an important by-product energy in steelmaking production, achieving the efficient recovery of which is greatly significant for energy saving and environmental pollution reduction in steelmaking process. However, the off-gas generated during steel production contains tremendous amounts of CO, which is

generally collected as a fuel to reheat the steel in rolling mills. Because a high concentration of CO (~15 vol.%) mixing with O_2 during pauses in the steelmaking process tends to cause explosions, the off-gas produced at this time is not directly recovered but is often discharged into the atmosphere via methane combustion-supporting flare burners [2].

Global requirement for a highly energy-efficient and low-carbon emission economy, particularly to reduce the emission of CO_2 by 2030 and carbon neutral by 2060 in China, depicts an essential effective combustion technology expected to utilize waste heat. To conserve the chemical heat from the discharged off-gas, we found that self-sustained catalytic combustion can be employed via the complete oxidation of CO, during which a CO/O_2 mixture generates local hot spots on the catalyst surface and adjacent CO and O_2 molecules are dissociated, followed by a thermochemical runaway reaction [3]. In this case, only a relatively small amount of energy is required for ignition since high temperatures are generated by the release of reaction heat without the need for external energy. The application of self-sustained catalytic CO combustion can be a potential strategy for electric power generation, with many advantages compared to conventional thermal combustion. On the one hand, the use of a catalyst permits the flameless combustion, with an enhanced combustion efficiency, of a fuel below its auto-ignition temperature in air. Consequently, the emission of NO_x is decreased as thermal-NO_x formation is limited due to lower combustion temperature [4]. On the other hand, catalytic combustion enables the burn-out of air/fuel mixtures well outside of the explosion limits (about

12.5–72.0 vol.% in air), leading to the broad security of energy recovery from diluted fuel streams [5]. It is obviously that the catalytic ignition of CO, as a complex process under the high CO concentration, includes kinetics and heat generation since the heat produced is governed by the reaction rate, which in turn is determined by the reaction kinetics [6-8]. Correspondingly, a transition from low-reactivity steady state to high-reactivity steady state can be observed due to heat transfer limitation. Such a strategy is thus different from current studies related to the slow reaction of CO at low concentration, which have focused on the reaction mechanism at a low-reactivity state, confined to the potential application needs.

Self-sustained catalytic combustion can be further enhanced if the employed catalytic material has a high activity. Supported noble metals are the typical used combustion catalysts, but they suffer from several drawbacks such as high costs and high-temperature sintering [9]. Another regularly researched catalytic system for the elimination of CO is the mixed metal oxide catalyst containing copper, cerium and zirconium, which is an alternative to noble metal catalysts offering the best compromise between cost, activity, selectivity, and thermal stability [10]. Here, the copper species are active and show a superior CO chemisorption. CeO_2 provides a large oxygen storage-release capacity because of the Ce^{4+}-Ce^{3+} redox couple, whereas doping Zr species into the CeO_2 lattice to form a Ce-Zr solid solution strongly affects the thermal stability of the catalysts [11, 12]. Furthermore, the Mars-van-Krevelen and Langmuir-Hinshelwood mechanism for CO oxidation, determined by specific catalyst, reactant concentration and reaction temperature, has been widely proposed

by using the traditional *in situ* DRIFT method [13,14].

To enhance the performances of mixed oxides for deep oxidation reactions, researchers have also attempted to fabricate binary oxides loaded onto highly porous nanoscale supports, such as nano-TiO_2, ZSM-5 zeolites and crystalline inorganic polymers, to improve the dispersion of the active sites. Francisco et al. [15] provided evidence that incorporating a minor amount of CuO into Ce/TiO_2 resulted in the maximum surface area value, where the presence of only two crystalline phases, anatase TiO_2 and CeO_2, promoted the dispersion of copper species. Li et al. [16] also confirmed that the active species CuO and the promoter Ce/Zr can be well dispersed over the ZSM-5 surface, and copper species mostly coexisted in the Cu^{2+} and Cu^{+} states, leading to a high activity. It is not surprising that heterogeneous catalysis is a complex process. Reactions occur on surfaces and at interfaces, where reactant molecules are adsorbed, activated, and converted into products that desorb into the gas phase [17, 18]. For the specific CO→CO_2 reaction over bulk Cu-Ce-Zr mixed oxides or those loaded onto TiO_2 and ZSM-5, the catalytic activity is not only determined by improving CO adsorption onto the dispersed copper sites but also depends on the oxygen vacancies, active oxygen properties, and mass and heat transfer rates, which can be tailored by the interactions among copper, cerium and supports (TiO_2 or ZSM-5) [19].

As a common and key issue, a better understanding of the support effects of TiO_2 and ZSM-5 on CO oxidation over $CuCe_{0.75}Zr_{0.25}O_{\delta}$ (CuCeZr), $CuCe_{0.75}Zr_{0.25}O_{\delta}/TiO_2$ (CuCeZr/T) and $CuCe_{0.75}Zr_{0.25}O_{\delta}$/ZSM-5 (CuCeZr/Z) is highly desired, but still

lacking. The research contribution of this work is mainly to investigate the interfacial synergy, which can result in unique geometrical, chemical or electronic properties that work either cooperatively or passively to enhance the activity and stability. The catalytic behaviors, including the ignition temperature, lean limit of combustion, wall temperature, heat output, and durability, were evaluated by the temperature-programmed oxidation (TPO) method, and then the structure of the catalysts was investigated by the state-of-the-art techniques. On this basis, the potential support effects on the reaction mechanism were investigated by FTIR coupled with a magnetically driven transmission cell, which is beneficially distinguished the formation of active intermediate peaks that are overlapped by the peaks of gaseous CO. Considering the self-sustained catalytic combustion of CO as a strong exothermic reaction, the present study also tries to investigate the influence of different catalysts to ignition temperature, self-sustained combustion limit, conversion efficiency, the wall temperature and heat output. The results obtained provide new insights into $CO \rightarrow CO_2$ efficient conversion and energy recovery with self-sustained catalytic CO combustion and are helpful for promoting the use of such technology for treating steelmaking off-gas.

2. Experimental

2.1. Synthesis of catalysts

The CuCeZr catalyst was synthesized by sol-gel method [7]. The CuCeZr/T and CuCeZr/Z catalysts were prepared using the incipient wet impregnation method,

where TiO_2 (P25, a mixture of the anatase and rutile phases) was supplied by Evonik Degussa and ZSM-5 (stoichiometric Si/Al ratio=25, crystallinity=100%) was supplied by Nankai University, Tianjin, China. The copper, cerium and zirconium nitrates (Kermel, Tianjin, China) with a Cu:Ce:Zr molar ratio of 1:0.75:0.25, were dissolved in deionized water and then mixed with TiO_2 (for the case of CuCeZr/T only) or ZSM-5 (for the case of CuCeZr/Z only). With respect to CuCeZr/T and CuCeZr/Z, the copper, cerium and zirconium contents were fixed at 4 wt.%, 6.6 wt.% and 1.4 wt.%, respectively. The actual loadings of copper, cerium and zirconium in each catalyst were measured by an inductive coupled plasma-optical emission spectrometry (ICP-OES, Agilent 720), as shown in Table 1, which is in good agreement with the theoretical content values as designed. The Cu:Ce:Zr molar ratio was selected based on our previous study, as the copper-cerium synergy at this ratio improved the redox capability and the formed cerium-zirconium solid solution also demonstrated a good oxygen storage capacity with this molar ratio [20]. The resulting solution was stirred at 80 °C for 24 h at a pH of approximately 7.0. After being dried by evaporation, the samples were calcined at 600 °C for 4 h to form the final catalysts.

2.2. Catalyst characterization

The specific surface areas of the catalysts were determined by nitrogen adsorption using a Quantachrom Nova 2000 apparatus. The BET specific surface areas were calculated from adsorption data acquired over a relative pressure (P/P_0) range of 0.05–0.25. The powder X-ray diffraction (XRD) analysis was carried out

using a XD-3-automatic (PERSEE) instrument with Cu Kα radiation (40 kV, 200 mA, λ = 1.5418 Å). The morphologies and phase purities of the catalysts were determined by scanning electron microscopy (SEM, Hitachi S4800) and transmission electron microscopy (TEM, PHILIPS Tecnai G^2 F20) coupled with Oxford-1NCA energy dispersive X-ray spectroscopy (EDX) detectors. X-ray photoelectron spectroscopy (XPS) was carried out on a Kratos Axis Ultra DLD spectrometer using an Al-Kα radiation source. The chemical states and surface compositions of the catalysts were examined by XPS analysis under the vacuum pressure (5×10^{-8} Pa) at ambient temperature rather than ambient pressure during CO oxidation in the heating process. Before the test, the samples were vacuumized to remove the moisture in the analyzer chamber. The purpose of the XPS measurements is to verify the existence of different Cu and Ce species (Cu^+, Cu^{2+}, Ce^{3+}, and Ce^{4+}) and obtain the ratios of them in the prepared catalysts. The binding energy was calibrated with the standard binding energy of C1 s (284.8 eV).

Temperature programmed reduction of hydrogen (H_2-TPR) measurements were carried out on a TP5080B chemisorption analyzer equipped with a thermal conductivity detector (TCD). Each sample (100 mg) was purged with He (30 mL/min) at 300 °C for 1 h and then cooled to room temperature. Finally, it was reduced under a flow of 10 vol.% H_2/He (30 mL/min) at a heating rate of 10 °C/min with a final temperature of 500 °C [21]. Temperature programmed desorption (O_2-TPD) measurements were obtained via the same instrument. The sample (200 mg) was pretreated at 500 °C for 30 min at He (30 mL/min), and then introduced O_2 (30

mL/min) for 1 h at room temperature. The TPD signal was monitored from room temperature to 950 °C at 10 °C/min under pure He.

To further investigate the CO adsorption and reactivity with O_2, *in situ* infrared spectroscopy experiments by using a Bruker Tensor 27 spectrometer coupled with a self-designed magnetically driven transmission cell (Tianjin Xianquan Industry and Trade Development Co., Ltd.) were also carried out. Because the optical path can be switched between the gas phase and catalyst by driving the quartz holder outside of the cell, the signals of the gas phase can be subtracted from the spectra at each tested temperature. This approach not only effectively eliminates the overlap of adsorption peaks in the gas phase but also enhances the signal-to-noise ratio at elevated temperatures. Approximately 40 mg of sample was pressed into the self-supporting wafer. Prior to the experiment, the sample was pretreated under a He flow (30 mL/min) at 400 °C for 1 h and cooled to room temperature for collection of a sample background spectrum. The reaction gas mixture (5 vol.% CO + 10 vol.% O_2, He balance) was fed to the sample at 30 mL/min. Here, the collection of a gaseous background spectrum was first achieved when the sample cell was pushed out the detection channel by connecting the magnetism handle at the desired temperatures and reaction atmosphere. Then the sample cell was quickly pushed into the detection channel to record infrared spectra of reactive intermediate species at corresponding temperatures with the same feed-gas conditions over the catalyst. For each temperature interval (from 50 to 300 °C), a series of time-dependent IR spectra of the reaction on the sample were sequentially recorded with a resolution of 4 cm^{-1} and the

accumulation of 64 scans.

2.3. Catalytic activity testing

The catalytic activity was evaluated in a flow-type apparatus designed for continuous operations at atmospheric pressure. Powdered catalyst (200 mg, particle size 0.15-0.3 mm) was packed into a quartz tube reactor with an inner diameter of 4 mm. To obtain the ignition temperature of the catalyst during self-sustained catalytic CO combustion, the feed gas was consisted of 10 vol.% CO + 10 vol.% O_2 + 80 vol.% N_2. Here, the used feed gas was below the explosive limit of CO (12.78-71.25 vol.%) [22]. In addition, contrasted to the gas-gas reactions by using a fire source in the CO + air atmosphere, CO catalytic combustion by temperature-programmed heating over the catalyst in a furnace belongs to the surface gas-solid reactions without a fire source, which also does not meet the explosion conditions. The total flow rate was fixed at 200 mL/min, corresponding to a weight hourly space velocity (WHSV) of 60,000 $mL \cdot h^{-1} \cdot g^{-1}$. The H_2O was introduced into the gas mixture by passing the gas stream through a gas saturator at 35 °C. The temperature programmed oxidation (TPO) experiment was carried out at a heating rate of 5 °C/min, and two K-type thermocouples (0.5 mm thick) were used. The first thermocouple was located before the catalyst bed to control the oven temperature along the flow, while the second thermocouple was inserted into the center of the catalyst bed to continuously monitor the temperature of the catalyst bed. On-line continuous analysis of the gaseous products was performed by nondispersive infrared absorption (QGS-08C for CO/CO_2,

Maihak) and a thermal conductivity analyzer (OGS-10T for O_2, Maihak), thus allowing evaluation of the CO conversion to CO_2 (CO_2 selectivity).

To determine the lean limit of self-sustained CO combustion, a reaction mixture of CO and air was fed into the reactor. The reactor was then electrically heated until the ignition of the reacting mixture occurred, as indicated by a steep increase in the temperature measured by the second thermocouple, where upon the heat supply was turned off and the reactor can be operated auto-thermally even when exposed to the atmosphere. An infrared camera (FLIR T640, USA) was employed to record the temperature distribution of the catalyst bed in each test. The infrared camera has a resolution of 640 × 480 pixels, a maximum frame rate of 30 Hz and a thermal sensitivity of 0.035 °C. For reproducibility, the self-sustained combustion was considered steady when the temperature of the reactor wall varies within a range of ±2 °C for 10 min, which is obviously higher than room temperature. The lean limit of combustion was defined as the CO/O_2 ratio, at which the energy generated by the combustion reaction was sufficient to maintain essentially complete conversion. Good reproducibility across three runs was found for the catalysts during each experiment.

3. Results and discussion

3.1. Catalyst structure and morphology

The morphologies and dimensions of the metallic particles of the CuCeZr/Z, CuCeZr/T and CuCeZr catalysts were evaluated using TEM analysis, as shown in Fig. 1. Pure ZSM-5 is commonly composed of irregularly localized, bright polycrystalline

aggregates with distinct edges [23]. For the CuCeZr/Z catalyst, small dark spots with sizes of less than 2 nm can be seen (Fig. 1a), which arise from a composition of Cu-, Ce- and Zr-rich phases based on the EDX elemental mapping results (point 1). The inhomogeneous distribution of Cu, Ce and Zr oxides (indicated with ellipses in Fig. 1a) suggests that a large fraction of these oxide clusters is located on the outer surface of the ZSM-5 crystals. The nanoparticles (NPs) of the tested TiO_2 are round and slightly aggregated, as seen in the TEM image of CuCeZr/T (Fig. 1b), while the grain sizes are within the range of 13–24 nm. The lattice fringes of the catalyst show d-spacings of 0.3516 and 0.3241 nm for TiO_2, which correspond to the (1 0 1) planes of anatase and (1 1 0) planes of the rutile phase, respectively. It is apparent that the Cu, Ce and Zr species are well dispersed according to the EDX results (point 2) in Fig.1e. The TEM images of CuCeZr (Fig. 1c) show that the CuO is agglomerated with a particle size of 4–12 nm. The formation of a Cu-Ce-Zr solid solution and crystalline CuO can be found by measuring the d-spacings (dCu-Ce-Zr solid solution (1 1 1) = 0.3125 nm and dCuO (1 1 1) = 0.2381 nm), which are smaller than that of a Ce-Zr solid solution (dCe-Zr (1 1 1) = 0.3149 nm) but higher than that of CuO (dCuO (1 1 1) = 0.2326 nm). This finding is consistent with the results of previous reports [24, 25].

Figure 1f presents the XRD patterns of the CuCeZr/Z, CuCeZr/T and CuCeZr catalysts. CuCeZr/Z shows sharp and intense peaks in the ranges of 8–9° and 22–25°, corresponding to a highly crystalline ZSM-5 structure. The XRD pattern of CuCeZr/T confirms the presence of the anatase crystal phase with high intensity peaks at 25.2°, 37.8°, 48.1°, 54.0°, 55.1°, and 62.8°, and the rutile phase with low intensity peaks at

28.7°, 36.8°, and 38.6°. The average crystallite size of the TiO_2 nanoparticles is ~21.3 nm based on the Debye–Scherrer equation. No diffraction peaks of copper, cerium or zirconium oxides are observed, which suggests that the Cu, Ce and Zr species are highly dispersed over the surfaces of the ZSM-5 and TiO_2 supports in the form of amorphous oxides or microcrystals. A typical cubic fluorite structure of CeO_2 can be observed in the XRD pattern of CuCeZr according to the peaks at 28.5° and 47.4°. The CuCeZr catalyst also shows two characteristic peaks of CuO at 35.5° and 38.7°. Compared to the diffraction pattern of cubic CeO_2, the diffraction peaks of CuCeZr are broadened and shifted to higher 2θ values, indicating the incorporation of copper and/or zirconium into the cubic fluorite structure of CeO_2.

The total surface areas of the catalysts are shown in Table 1. For CuCeZr/Z, the surface area decreased from 376.3 m^2/g to 346.3 m^2/g after Cu, Ce and Zr species were incorporated into ZSM-5. The decreased surface area could be linked to some of the pores of ZSM-5 being blocked or the external surface of ZSM-5 being covered by the Cu, Ce and Zr species. It is well known that ZSM-5 is a crystalline inorganic polymer with a good pore structure, consisting of a three-dimensional (3-D) network of SiO_4 and AlO_4 tetrahedra linked by interconnecting oxygen ions. By contrast, TiO_2 does not have such a good pore structure. Hence, compared with the commercial Degussa P25 TiO_2 (176.8 m^2/g), the well dispersion of Cu, Ce and Zr species on the TiO_2 surface slightly decreased the surface area of CuCeZr/T (168.2 m^2/g). In comparison, CuCeZr shows the lowest surface area (30.5 m^2/g) among the catalysts. This can be mainly attributed to the formation of a larger amount of oxide crystals

after the calcination process, as determined by XRD.

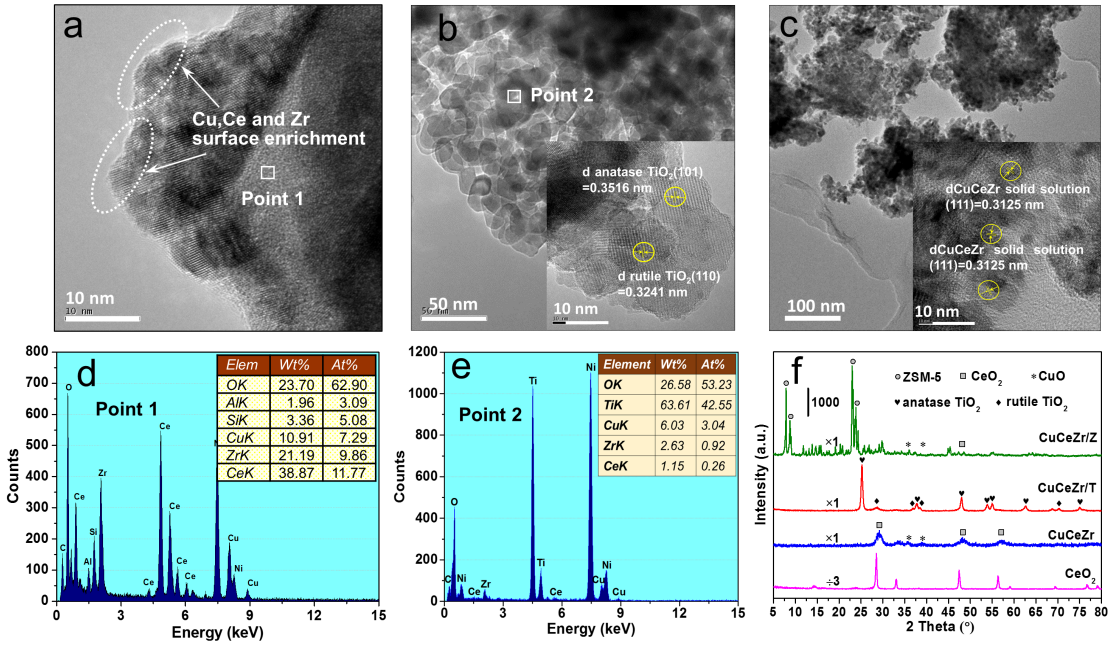

Fig. 1. TEM images + EDX spectra of CuCeZr/Z (a, d), CuCeZr/T (b, e), CuCeZr (c) and XRD patterns (f) of catalysts.

Table 1 The BET surface areas and elemental contents of catalysts.

Sample	Surface area (m^2/g)	Elements content (wt.%)		
		Cu	Ce	Zr
ZSM-5	376.3	--	--	--
TiO_2	176.8	--	--	--
CuCeZr/Z	346.3	4.2	6.5	1.6
CuCeZr/T	168.2	4.1	6.4	1.6
CuCeZr	30.5	25.6	43.7	5.9

3.2. Surface chemical states and chemisorption

The chemical states and surface compositions of the catalysts were

investigated by XPS analysis. As shown in the core-level spectra of Cu $2p_{3/2}$ (Fig. 2a), the shake-up peaks at ~944 eV is observed for all the catalysts, confirming the presence of copper ions in the 2+ oxidation state. However, the asymmetry and the shift of the peak maxima of the Cu $2p_{3/2}$ main peak reveals the contributions from copper ions in oxidation states below 2+ [26]. The Ce 3d core-level spectra (Fig. 2b) show the "v" and "u" peaks corresponding to the $3d_{5/2}$ and $3d_{3/2}$ states, respectively. The doublets (v, u), (v'', u''), and (v''', u''') can be assigned to the various states of the Ce^{4+} ions, whereas the doublet (v', u') represents the Ce^{3+} species [27, 28]. Thus, Ce^{3+} and Ce^{4+} species coexist in each catalyst. It has been reported that the presence of more Ce^{3+} in the catalysts favors the formation of vacancies and unsaturated chemical bonds on the catalyst surface [29]. As a surface technique, XPS preferentially detects species located on the surface of the sample (a sampling depth within the range of 3-10 nm). The surface elemental compositions were calculated according to the relative peak areas of the XPS spectra (Table 2). The copper and cerium contents of CuCeZr/T appear to be enriched on the surface of TiO_2 compared to those of ZSM-5, although both catalysts have the same bulk composition, indicating that numerous copper and cerium species are located within the ZSM-5 channels. The Cu/(Ce+Zr) atomic ratio is similar for all the catalysts, but the Ce/Zr atomic ratio for CuCeZr/T and CuCeZr is 1.8 and 4.1, respectively, which is larger than that of CuCeZr/Z (0.7). The enrichment of cerium on the surface of the Ce-Zr solid solution is favorable to promote the oxygen cycle, especially a relative high ratio of Ce^{3+}/Ce^{4+} for CuCeZr/T. Quantitative analysis also gives a Cu^{2+}/Cu^{+} ratio of 1.7 for CuCeZr/T, 3.4 for

CuCeZr/Z, and 0.6 for CuCeZr, indicating that copper exists mostly in a univalent oxidation state on the CuCeZr. More Cu^{2+} ions were found in CuCeZr/T and CuCeZr/Z than in CuCeZr, which can be associated with the copper ions that are highly dispersed over the TiO_2 and ZSM-5 supports, thereby being more exposed and easily oxidized during the calcination process.

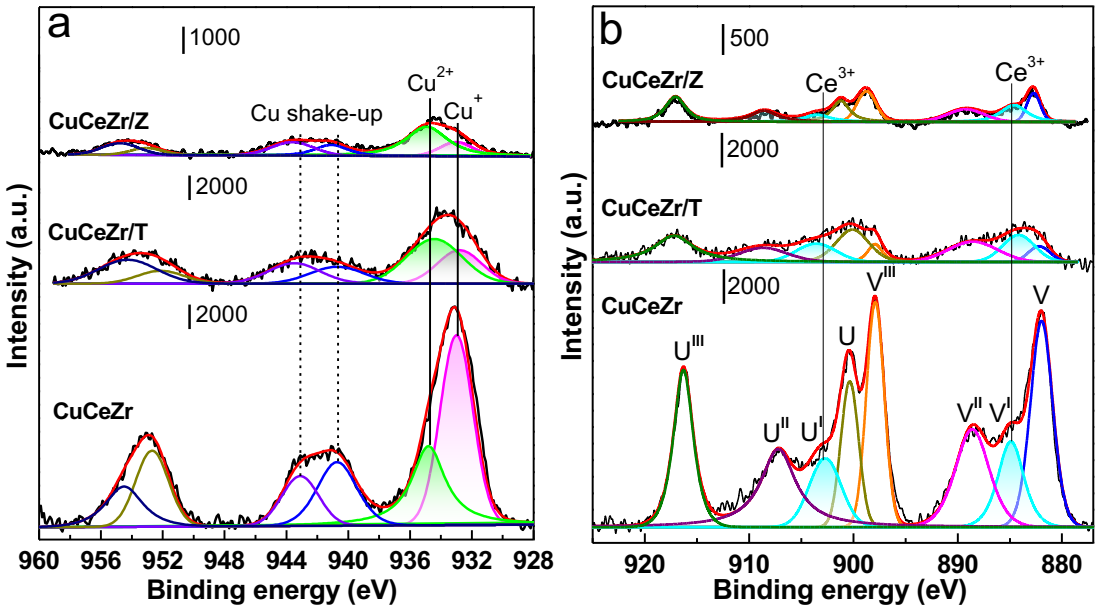

Fig. 2. XPS narrow spectra of Cu 2p (a) and Ce 3d (b) of CuCeZr/Z, CuCeZr/T and CuCeZr catalysts.

Table 2 Surface composition of catalysts derived from XPS analysis.

Sample	Surface element composition (at.%)							Cu/(Ce+Zr)	Ce/Zr	Ce^{3+}/Ce^{4+}	Cu^{2+}/Cu^{+}
	Cu	Ce	Zr	O	Si	Al	Ti				
CuCeZr/Z	3.8	1.4	2.1	32.7	14.3	0.4	/	1.1	0.7	0.22	3.4
CuCeZr/T	5.4	3.1	1.7	37.1	/	/	10.8	1.1	1.8	0.36	1.7
CuCeZr	15.1	8.9	2.2	51.3	/	/	/	1.4	4.1	0.21	0.6

The redox ability and quantitative analysis of copper species were studied using H_2-TPR. A high total H_2 consumption together with a low reduction temperature is

related to the active sites available for CO oxidation that promote the activity of the oxygen cycle. It is well known that the H_2 consumption is mainly contributed by Cu species in the prepared catalysts at reaction temperatures of 50-500 ºC [8]. Within the range of reducing temperatures, the profile of CuCeZr (Fig. 3a) exhibits two reduction peaks, α (200 °C) and β (253 °C), corresponding to the reduction of Cu species of the Cu-Ce solid solution (Cu-[O_v]-Ce), surface dispersed CuO and crystallized CuO, respectively. Compared with CuCeZr, the CuCeZr/T catalyst shows two reducing peaks with lower intensity at 210 °C and 334 °C due to its low content of copper, cerium and zirconium. The low temperature peak (α) can be assigned to the reduction of copper in the highly dispersed CuO NPs because of its interaction with the TiO_2 support. The high temperature peak (β) is associated with CuO bound to TiO_2, which is unreducible. Li et al. [30] reported similar results regarding the β peak, deducing that CuO interacts with the surface hydroxyl groups of TiO_2 to form a new structure that anchors CuO onto the surface of the TiO_2 support. For CuCeZr/Z, the reduction of H_2 can be split into two general peaks, which correspond to the reduction of highly dispersed CuO NPs supported on ZSM-5 (α peak, 199 °C) and isolated copper ions incorporated into the framework of the zeolite structure (β peak, 270 °C), respectively [31]. Combined with the XRD analysis, the wide span of the α peak suggests that the CuO microcrystals possess a diverse range of sizes, which interact disparately with the support, leading to the consumption of hydrogen over a wider range of temperatures [32].

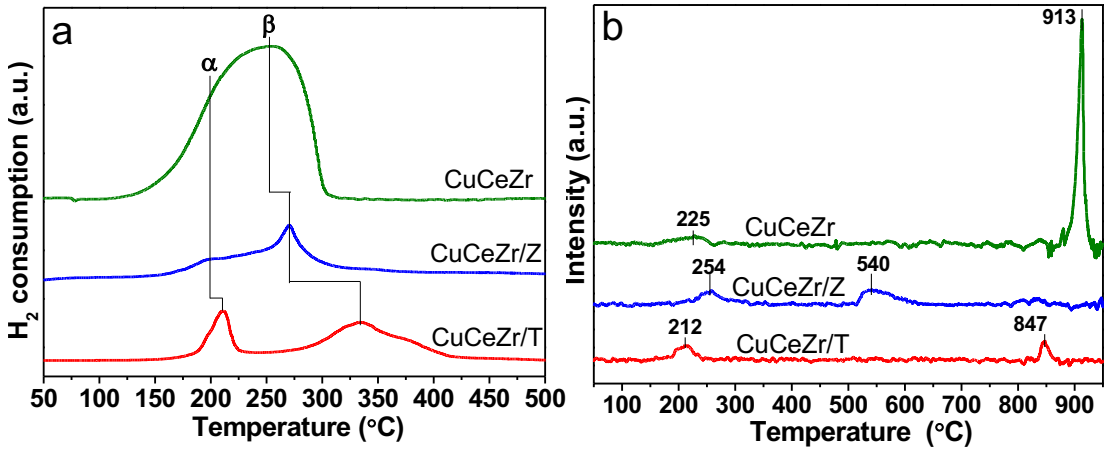

Fig. 3. H_2-TPR profiles (a) and O_2-TPD profiles (b) of CuCeZr/Z, CuCeZr/T and CuCeZr catalysts.

Table 3 Hydrogen consumption and O_2 desorption of CuCeZr/Z, CuCeZr/T and CuCeZr catalysts.

Sample	H_2 consumption (μmol/g)	O_2 desorption (μmol/g)	
		O_A	O_L
CuCeZr/Z	179	14.3	16.5
CuCeZr/T	414	9.2	3.9
CuCeZr	1305	8.2	52.5

Table 3 summarizes the total amounts of H_2 consumed using different catalysts. As expected, the total amount of H_2 consumption for CuCeZr was 1305 μmol/g, higher than those of CuCeZr/T and CuCeZr/Z due to the higher copper loading of CuCeZr, which is also confirmed by the ICP-OES analysis (Table 1). Combined with the TEM results (Fig.1), XPS results (Fig.2) and BET surface areas (Table 1), the vast majority of copper species are well dispersed on the TiO_2 surface of CuCeZr/T and

then exhibit a moderate H_2 consumption amount. Because of the parts of copper species are located in the ZSM-5 channels blocking the micropores of ZSM-5, thus, they are difficult to be reduced by hydrogen, leading to the lowest H_2 consumption. The redox properties of the copper species decrease according to their reduction temperatures and H_2 consumptions in the following order: CuCeZr > CuCeZr/T > CuCeZr/Z. With respect to CuCeZr, the low temperature α peak suggests its enhanced catalytic reducibility, which might be attributed to numerous copper ions being incorporated into cerium to form a solid solution, as confirmed by the XRD and TEM analysis, thus weakening the Cu-O and Ce-O bonds.

O_2-TPD analysis was used to understand the formation of the oxygen species and oxygen mobility (Fig. 3b and Table 3). Both surface adsorbed oxygen O_A (< 450 °C) and lattice oxygen O_L (> 450 °C) were detected for all the catalysts. It is important to note that the structure of CuCeZr and the supports (ZSM-5 and TiO_2) can significantly affect the oxygen adsorption and desorption ability. The O_2-TPD profile of CuCeZr shows a peak at approximately 110–250 °C, which is related to the weak desorption of surface oxygen species, while the intense peak above 750 °C can be attributed to the desorption of lattice oxygen. The quantity of surface adsorbed oxygen tends to increase with increasing specific surface area since the presence of ZSM-5 and TiO_2 supports lowers the formation of lattice oxygen but increases the amount of surface adsorbed oxygen, especially for CuCeZr/Z.

3.3 CO catalytic ignition and long-term stability testing

The catalytic activities of the catalysts were evaluated using TPO (gas composition of 10 vol.% CO + 10 vol.% O_2 + 80 vol.% N_2 and a flow rate of 200 mL/min), and the transient curves for CO ignition are presented in Fig. 4a. For example, for CuCeZr/Z without any preheating, the temperature is equal to the inlet temperature of 20 °C, and no CO conversion is observed. Increasing the furnace temperature increases the CO conversion to CO_2 at a relatively slow rate, reaching ~5.0% at 169 °C. This induction process is kinetically dominated, as reflected by the temperature of the catalyst bed being close to that of the furnace. As a typical fuel-rich mixture, the equivalence ratio Φ of the CO-O_2 mixture is 0.26, defined as the CO-to-O ratio in the feed gas divided by the stoichiometric ratio necessary for complete CO combustion. In this case, the CO ignition occurs at the gas-solid interface. The system correspondingly transitions to a condition with high CO conversion, leading to a significant increase in the maximum of reaction temperature. Entering this step indicates that the reaction rate is controlled by internal diffusion [33]. The ignition temperature (T_{ig} = 175 °C) is the temperature beyond which the system transitions to the ignition reaction, and is determined from the temperature achieving 50.0% CO conversion. Complete conversion of CO was observed after the remarkable runaway of the reaction, where the reaction rate was controlled by external diffusion [34]. Because the rapid mass and heat transfer at the gas-solid interface promotes self-sustained combustion, full CO conversion can be consistently sustained even after switching off the heating, and the hot-zone temperature in the

catalyst bed remains at 446 °C. These three catalysts show a similar ignition profile but different T_{ig} values: 175 °C for CuCeZr/Z, 146 °C for CuCeZr/T and 63 °C for CuCeZr. Hence, the reaction activity for the CO catalytic ignition follows the order: CuCeZr > CuCeZr/T > CuCeZr/Z. Evidently, a low ignition temperature is more favorable for ignition procedures with fast responses and can avoid the need for auxiliary devices such as preburners, eliminating their additional contributions to pollutant formation. After adding 5 vol.% H_2O over the superior CuCeZr, the curve of the activity shifts toward higher temperatures (T_{ig}=76 °C) and thus inhibits catalytic performance slightly. But the CO can be completely converted to CO_2 via $2CO+O_2 \rightarrow 2CO_2$, with the same change tendency as that without H_2O addition.

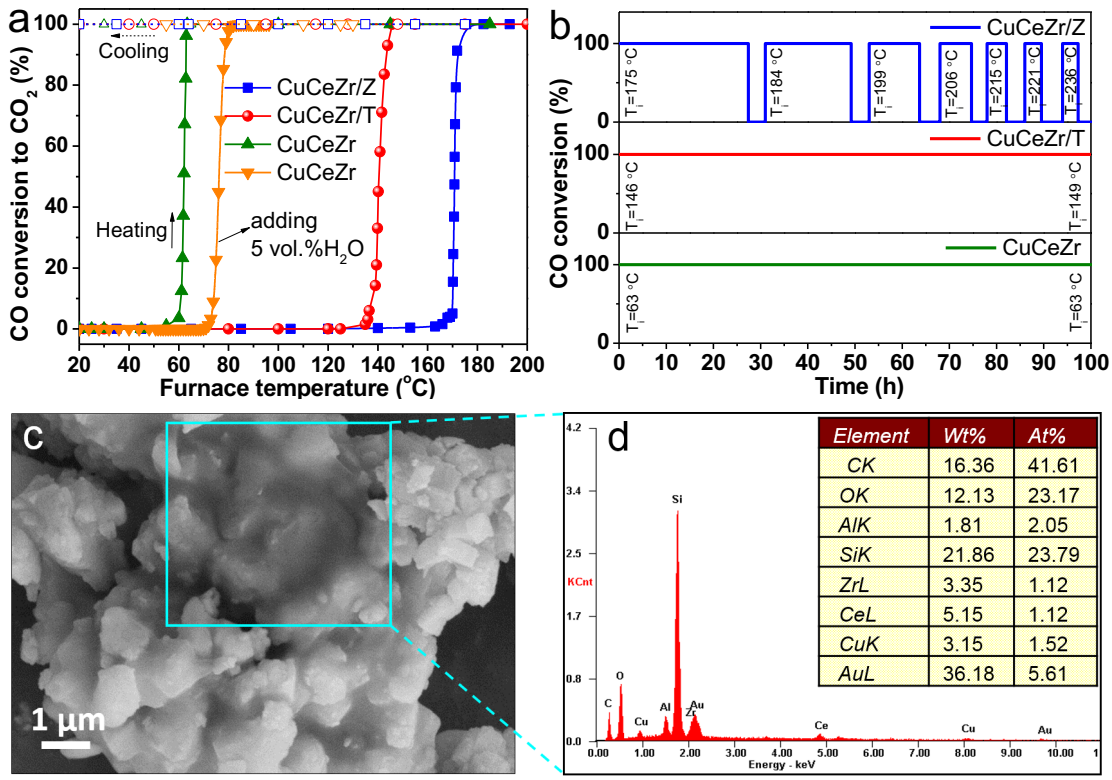

Fig. 4. Catalytic performance of all the catalysts: ignition curves (a), time-on-stream behaviors (b); SEM image (c) and EDX spectrum (d) of carbon deposition over inactivated CuCeZr/Z catalyst after a six-cycle durability test.

A time-on-stream study was carried out to assess the catalyst stability using 10 vol.% CO + 10 vol.% O_2 + 80 vol.% N_2 at a flow rate of 200 mL/min. Figure 4b clearly shows a stable CO combustion over CuCeZr during the 100-h experiment. Likewise, a stable catalytic performance is observed over 100 h with almost no change in the CO conversion when using CuCeZr/T, although T_{ig} slightly shifts to 149 °C (146 °C for the fresh catalyst) when the system is restarted after the 100-h test. Under the same conditions, however, the self-sustained combustion of CO over CuCeZr/Z can be maintained for only 27.4 h, after which the deactivation of the catalyst took place, evidenced by a rapid decline in the CO conversion. Although we restarted the reaction after a 2 h regeneration of the CuCeZr/Z catalyst at 600 °C under an air atmosphere, the self-sustained combustion of CO lasted for only 19.2 h, and the CuCeZr/Z catalyst was deactivated again. This deactivation was accelerated after six cycles of catalytic reaction and catalyst regeneration, corresponding to the continuous running time being reduced to 3.3 h and T_{ig} increasing to 236 °C. Clearly, among the three catalysts tested, bulk CuCeZr exhibits excellent activity and stability for self-sustained CO combustion, and thus showing a great potential for industrial applications. The closed interactions of Cu and Ce leading to the formation of Cu-Ce solid solutions in CuCeZr is the major contribution to superior activity. The support effects involving that CO oxidation mainly occurs at the phase interface between the copper oxides and TiO_2/ZSM-5 over CuCeZr/T and CuCeZr/Z, which also confirmed by the following *in situ* Infrared results. The TiO_2 and ZSM-5 supports promote the dispersion of copper species, particularly for TiO_2, resulting in a higher activity of

CuCeZr/T than CuCeZr/Z.

To probe the nature of the deactivated catalysts, SEM/EDX was further performed on the spent catalysts. SEM images of CuCeZr/Z (Fig. 4c) show that the surface is partially covered by a layer of coke (16.36 wt.%,) as determined quantitatively by the EDX characterization (Fig. 4d). However, such a phenomenon was not found on the CuCeZr and CuCeZr/T catalysts. This is not surprising considering that the carbon species are distributed over both the copper sites and acidic functional sites of the CuCeZr/Z catalyst, resulting in a rapid deactivation. The deactivation of ZSM-5 by coking was also studied in the literatures [35] [36], where coke was formed via the strong adsorption of its precursors onto the Brønsted acid sites, resulting in the condensation and rearrangement reactions of these compounds.

3.4. Stability limit of self-sustained catalytic CO combustion

Wider stability limits are desirable to achieve a higher CO/O_2 mixing ratio for the self-sustained combustion of CO as well as the ignition of catalytic combustors at low temperatures. Figure 5a displays the profiles of the combustion stabilities, exhibiting a V-shape for all the catalysts. At a flow rate of < 200 mL/min, a lower equivalence ratio Φ leads to a lower amount of released heat. A higher heat loss ratio in this case is unfavorable for stabilizing the hot points on the catalyst surface and maintaining the self-sustained catalytic combustion of CO. When the flow rate is higher than 200 mL/min, the hot points are unsustainable with a continuously increasing the flow rate, followed by increasing CO exiting the outlet without burning, which can also lead to

higher heat losses. At the same flow rate, the stability limits reflected by the Φ values of the catalysts are related to their activities (ignition temperatures) following the order CuCeZr > CuCeZr/T > CuCeZr/Z. Figure 5b-d displays a two-dimensional temperature distribution of the reactor in the self-sustained CO catalytic combustion, where the Φ value for each test is determined according to the limits of self-sustained combustion as shown in Fig. 5a. Heat and mass transfer occur in the catalytic combustion since the packed bed is cooled at the walls. Hence, the centerline tends to be hotter than the walls, and reactants are more rapidly consumed there, making the reaction faster.

Figure 5e depicts the temperature distributions of the axial wall obtained according to Fig. 5b-d. The temperature gradient near the inlet is initially steep and reaches a hot zone located within the packed catalyst bed, after which the temperature gradually decreases in the flow direction because of the competition between heat release and heat loss. The entire temperature profile shifts downstream with increasing the flow rate, particularly for the CuCeZr/Z and CuCeZr/T catalysts, resulting in higher exhaust gas temperatures and significant heat losses. At the same flow rate, CO starts to react at the later stages of the catalyst beds comprising CuCeZr/Z or CuCeZr/T. Due to the inadequate number of active sites per unit of catalyst, a higher temperature and longer reaction time are required for CO ignition in this case. For CuCeZr, however, CO can be oxidized rapidly near the inlet, where the intense heat does not need to react along the gas flow.

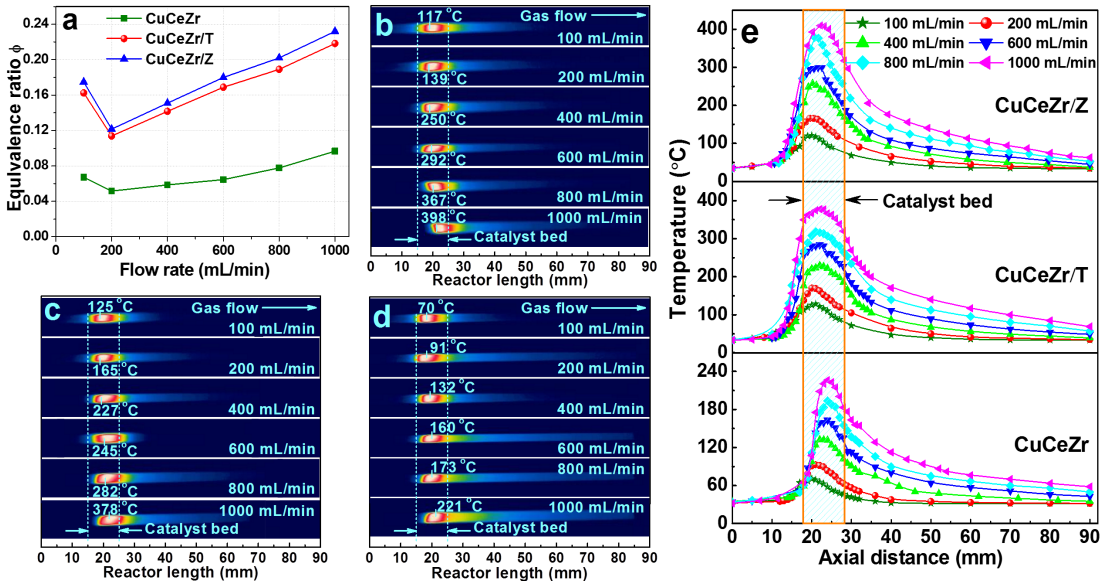

Fig. 5. Φ limits of CO self-sustained combustion at CO lean conditions (a), Two-dimensional temperature distribution in reactor for the CuCeZr/Z (b), CuCeZr/T (c) and CuCeZr (d) catalysts, and Variation in the axial temperature profiles (e) along the combustion chamber using different catalysts.

The heat transfer balance can be maintained during a stable self-sustained catalytic combustion over the catalysts, where the loss of heat transfer between the outer walls and ambient environment can be calculated [37]. As shown in Fig. 6a-c, the total heat released (Q_{gen}), the heat transfer rate of free convection (Q_c) and radiation (Q_r) exhibit upward trends upon increasing the flow rate. As a result of the high Φ values obtained over CuCeZr/Z and CuCeZr/T, the values of Q_{gen}, Q_c, Q_r are higher than those of CuCeZr, but this corresponds to a relatively lower surface heat loss rate per unit of generated power (η) (Fig. 6d).

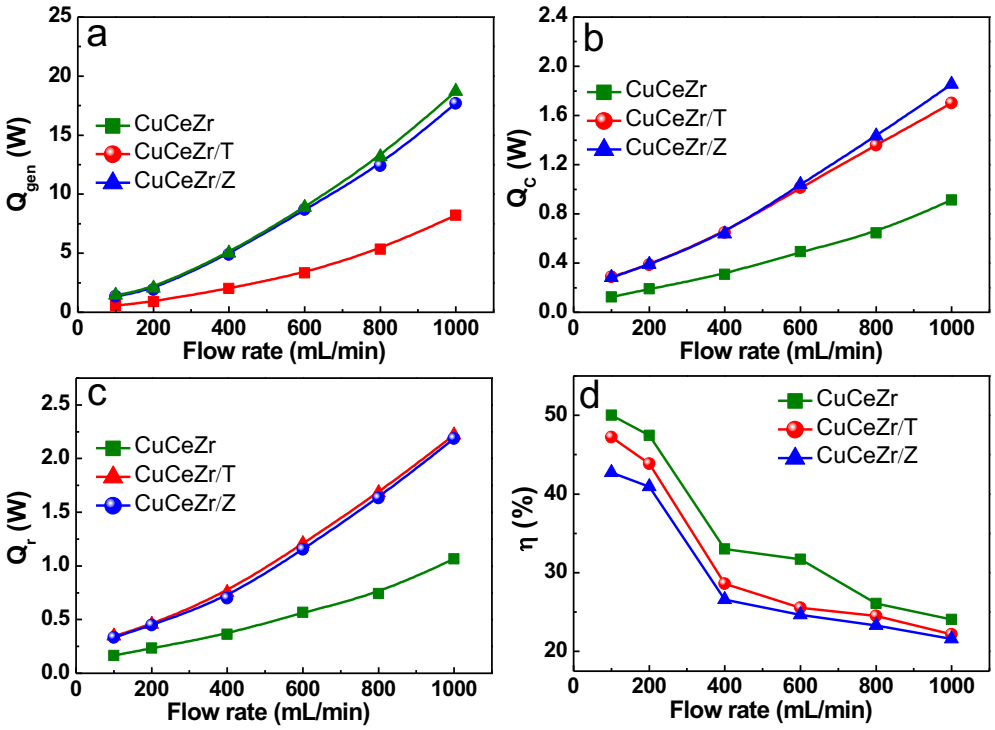

Fig. 6. The heat transfer versus flow rate over the catalysts: total released heat (a), heat transfer rate of free convection (b), radiation (c) and surface heat loss rate (d) per unit of generated power.

3.5. Proposed reaction pathways

The *in situ* infrared reactor was designed with a magnetically driven transmission cell, which is beneficially distinguished the formation of active intermediate peaks and gaseous CO peaks (Fig. 7a). A gaseous background spectrum can first be collected by pushing the sample cell out the detection channel and attaching the magnetism handle at the proper temperatures and reaction atmosphere. The sample cell was then quickly pushed into the detection channel, where infrared spectra of reactive intermediate species at corresponding temperatures under the same reaction conditions were recorded over the catalyst. The similar method was also reported to subtract gas-phase background [38]. It should be noted that the active sites and

intermediates of reaction pathways over catalysts were analyzed based on both the variation of formed apparent intermediate adsorbed species and CO_2 yield, because the majority of true intermediates are more likely to react with a high turnover frequency and produce gaseous CO_2 quickly at desired temperatures in the CO oxidation reaction. *In situ* infrared spectroscopy was used to probe the formation of surface Cu ion adsorption sites and the oxidation behavior of CO over different catalysts (Fig. 7b-d). Considering that the CO and CO_2 contributions from atmosphere have been subtracted from the spectra for each temperature tested, bands can be observed to basically form in three spectral zones that generally relate to the gaseous CO_2 (2382-2310 cm^{-1}) produced at different reaction cell temperatures, the formation of carbonyl species (2200-2000 cm^{-1}) and the formation of carbonate, carboxylate or formate species (1800-1200 cm^{-1}). The catalytic activity of copper-cerium-based materials toward CO oxidation is largely affected by two significant factors: the Cu ion active sites and the surficial active oxygen species [39].

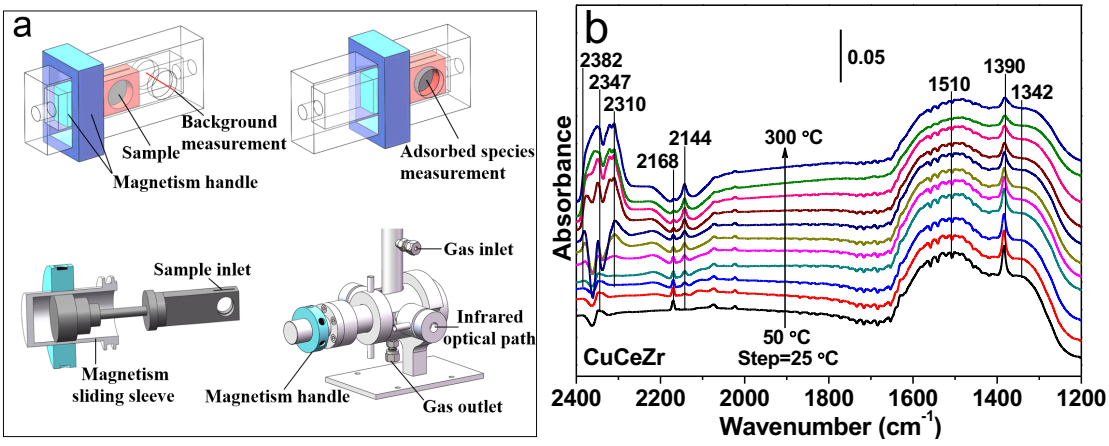

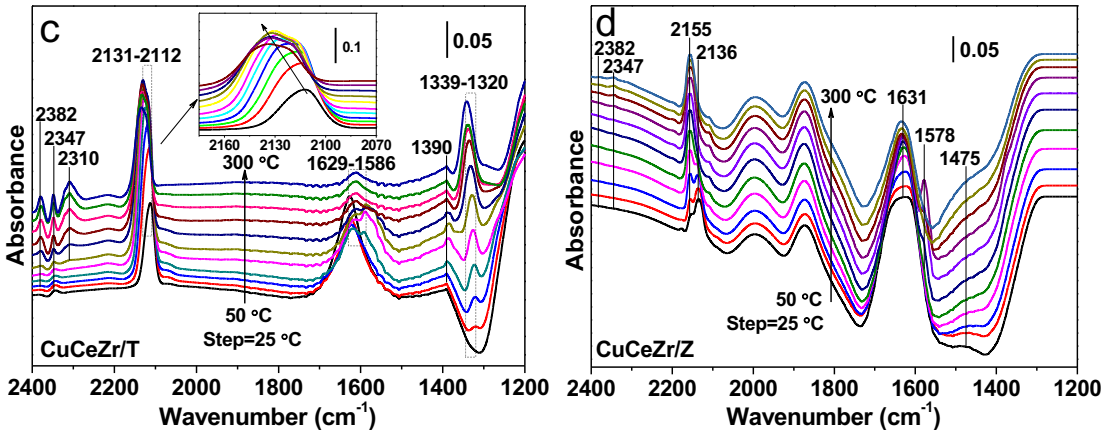

Fig. 7. Schematic diagram of the *in situ* infrared with a magnetically driven transmission cell (a) and *in situ* infrared spectra for the CO oxidation over CuCeZr (b), CuCeZr/T (c) and CuCeZr/Z (d) catalysts under 5 vol.% CO + 10 vol.% O_2 + 85 vol.% He continuous stream conditions.

When gaseous CO is first coordinated to copper cationic centers to form carbonyls, the C-O stretching frequency shifts compared to that of the original CO measured in the gas phase (2172 and 2112 cm^{-1}). The [Cu^{+}-CO] carbonyls exhibit higher stability due to the synergy between the σ bonds and π-back-bonding between CO and copper cations. In contrast, the [Cu^{2+}-CO] species are labile since the bonds have σ characteristics, whereas the [Cu^{0}-CO] carbonyls have low stability related to the weak σ bonds and π-back-bonding. Therefore, for CuCeZr, the band at 2144 cm^{-1} in Fig. 7b can be assigned to CO adsorption onto Cu^{+} to form a monocarbonyl complex [Cu^{+}-CO] [40] since the d-orbitals of the Cu^{+} cations are completely filled (an outer-shell electron distribution of 3d10) and thus can form strong bonds with CO. The assignment of the 2168 cm^{-1} band is less straightforward. Hornés et al. [41] noted that the band at 2176-2167 cm^{-1} can be attributed to CO adsorbed onto unsaturated Ce^{4+} cations, based on parallel CO-TPR experiments, but the [Ce^{4+}-CO] carbonyls are formed at temperatures > 230 °C. Our previous work reported that no bands relating

to [Ce^{4+}-CO] are produced at room temperature as the cerium ions, with an outer-shell electron distribution of 5s2 4d10 5p6, do not readily donate electrons from their d-orbitals to the antibonding π-orbitals in such a situation [42]. Consequently, the band at 2168 cm^{-1} might be induced by CO adsorption onto the oxygen vacancies of the interface between the copper and cerium oxides to form a [Cu^{+}-(C≡O)-Ce^{3+}] species [43]. The oxygen vacancies occupied by CO lead to self-poisoning of CO and then react with active lattice oxygen at low temperature, and the proposed reaction pathways are shown in Fig. 8a. CO can also be chemisorbed onto the cerium components, forming carboxylate (1510 cm^{-1}), formate (1390 cm^{-1}) and carbonate (1342 cm^{-1}) species, followed by the production of reduced cerium. However, the amount of carbonate species formed through the interaction of CO with pure copper oxides is practically zero at room temperature [44, 45]. Increasing temperature leads to a rapid decrease in the intensity of the band at 2168 cm^{-1}. Meanwhile the intensity of the bands at 1510, 1390 and 1342 cm^{-1} decrease slowly with rising temperature, which corresponds to a relatively low yield of CO_2. However, significant production of CO_2 mainly occurs via the formed abundant [Cu^{+}-CO] species reacting with active lattice oxygen at high temperatures of > 200 °C (Fig. 7b and 8a). Here, the ignition temperature in the IR cell is higher than that in the powder-filled tube reactor, suggesting that the pressed-powder wafer is unfavorable for the accumulation of heat during the exothermic reaction. These findings suggest that the formation of [Cu^{+}-CO] species is a major contributor to CO ignition, considering the intensity of the band at 2144 cm^{-1} increases at the expense of the decreased intensity of the band at 2168 cm^{-1},

and the interface vacancies being occupied by oxygen rather than CO indicates the acceleration of the oxygen cycles. Therefore, as shown in Fig. 8a, CO first adsorbed onto the oxygen vacancies at the interface between the Cu and Ce oxides to form [Cu^{+}-(C≡O)-Ce^{3+}] at low temperatures. In addition to the inactive carbonates, the monocarbonyls [Cu^{+}-CO], which are more likely to replace [Cu^{+}-(C≡O)-Ce^{3+}] at high temperatures, are the dominant active species to react with lattice oxygen for CO oxidation, and the vacancies occupied by oxygen accelerate the oxygen cycles.

Using TiO_2 or ZSM-5 support enhanced the dispersion of Cu species on the CuCeZr/T and CuCeZr/Z catalysts. The high surface areas (Table 1) of the supports seem to play major roles, while the Cu-Ce interactions seem to be less relevant. Similar to that of CuCeZr, CO is also adsorbed onto the copper sites to form carbonyls. The existence of Ce^{3+} on the catalysts favors oxygen vacancies formation. In Fig. 7c and 7d, clear redshifts of the carbonyl peaks for CuCeZr/T (2131 and 2112 cm^{-1}) and CuCeZr/Z (2155 and 2136 cm^{-1}) are observed compared with CuCeZr, which can be attributed to the support effects of TiO_2 and ZSM-5, especially the former. Furthermore, the corresponding intensities of the carbonyl peaks distinctly increase. This IR signal shifting is determined by the contributions of both the σ-bonds and π-back-bonds. When only a σ bond is formed, the stability of the carbonyls increases with increasing effective positive charges of the cations, which corresponds to a blueshift of the C-O vibration. The π-back-bonding forms at the expense of the electron transfer from the d-electrons of the Cu^{+} cations to the $2\pi^*$ antibonding orbitals of the CO molecules, corresponding to a redshift [46]. Evidently,

compared with CuCeZr, the synergy between π-back-bonding enhancement and σ-bond weakening in CuCeZr/T and CuCeZr/Z leads to strengthen the Cu-C bonds but decreases the C-O bond order, which favors CO oxidation. Of particular interest are the transformations of the carbonyls upon increasing the temperature (2112→2131 cm^{-1} for CuCeZr/T and 2136→2155 cm^{-1} for CuCeZr/Z), where the peaks at 2112 and 2136 cm^{-1} can be assigned to monocarbonyls [Cu^{+}-CO] while the peaks at 2131 and 2155 cm^{-1} are attributed to dicarbonyls [$Cu^{+}(CO)_2$]. The increase of dicarbonyl signal with increasing temperature can be explained by the successive reduction of agglomerated Cu^{2+} species with less support effect to form Cu^{+} cations. The intensities of the dicarbonyl signals are positively correlated with the enrichment of Cu^{2+} cations on the support determined by XPS. Dang et al. [47] and Yan et al. [48] considered that the reduction of Cu^{2+} by CO requires the existence of oxygen attached to the copper sites. Consequently, the Cu^{+} created by the interaction of the sample with CO at elevated temperatures indicates the presence of oxocation species such as [Cu^{2+}-O-Cu^{2+}] [49]. After the reduction by CO, isolated Cu^{+} sites are formed onto which CO can be subsequently adsorbed [50]. The dicarbonyls formed after CO chemisorption prevail on the surface as the major components of CO oxidation, are more active than the carboxylate (1390 cm^{-1}) and formate (1339-1320 cm^{-1}) species of CuCeZr/T and the carbonate (1578, 1475 cm^{-1}) species of CuCeZr/Z, and react with active oxygen to produce CO_2. Hence the monocarbonyls [Cu^{+}-CO] should be firstly reacted with lattice oxygen at low temperature and the dicarbonyls [$Cu^{+}(CO)_2$] are acted as the main intermediates at high temperatures for CO oxidation for CuCeZr/T

and CuCeZr/Z (Fig. 8b and 8c).

As the CO molecules are chemisorbed onto the ZSM-5 surface followed by the dissociation on the catalyst surface, the coke deposition occurs primarily at the Brønsted acid sites linked to the framework aluminum atoms, but with a non-negligible contribution from Lewis acid sites (Fig. 8c). Characteristic hydrogen carbonate peaks are also observed at around 1631 cm^{-1} (Fig. 7d), which should be located at the Al^{3+} sites, followed by the condensation and rearrangement reactions of these compounds. By comparison, CO molecules adsorbed onto the Ti^{4+} sites can also form hydrogen carbonates on CuCeZr/T (1629-1586 cm^{-1}, Fig. 7c) [51], which can be easily eliminated by the self-exothermic CO oxidation reactions.

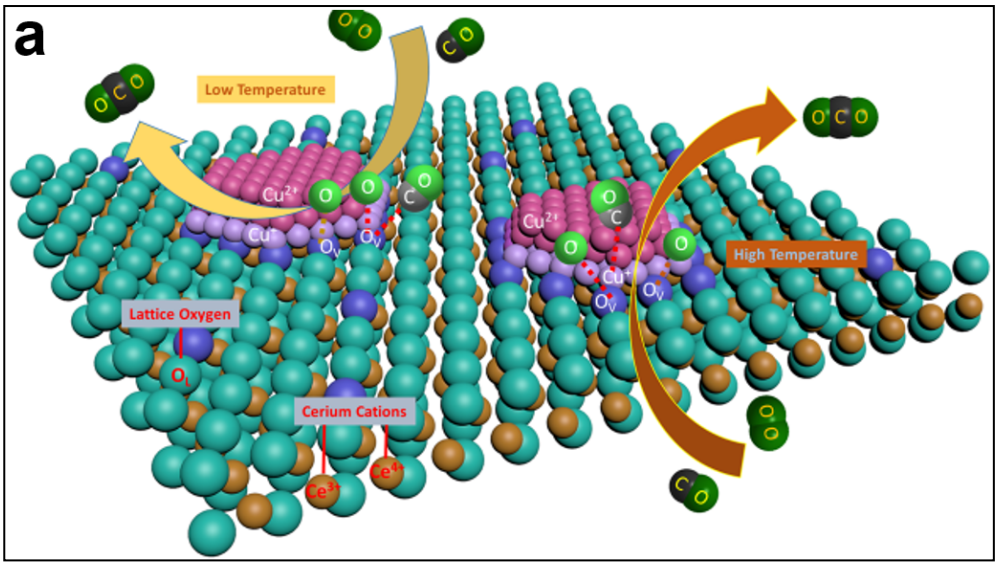

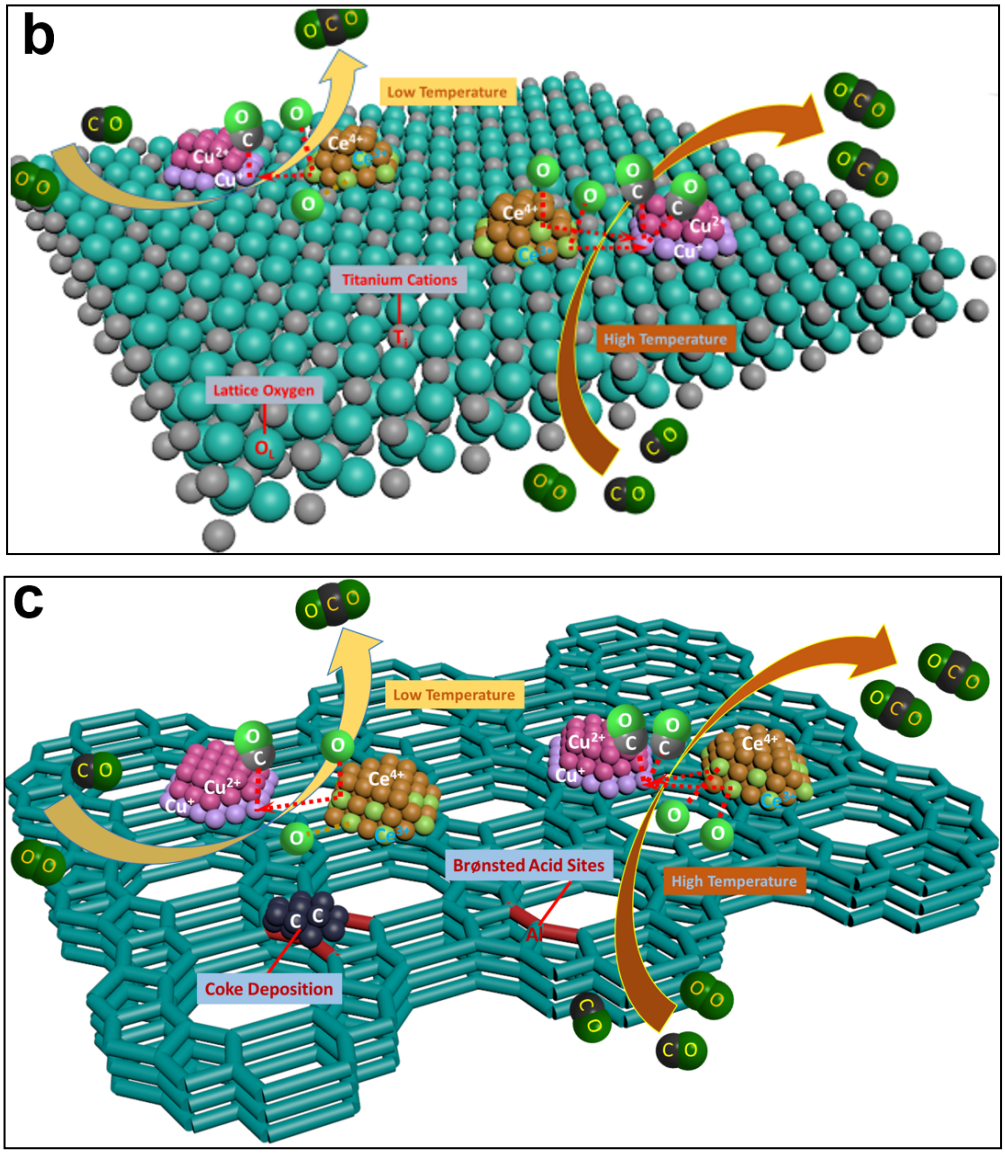

Fig. 8. Possible reaction mechanisms of catalytic ignition of CO over the CuCeZr (a), CuCeZr/T (b) and CuCeZr/Z (c) catalysts.

4. Conclusions

This study highlighted the support effects and reaction pathways on the catalytic ignition of CO and their stabilizing roles for bulk CuCeZr, CuCeZr/Z and CuCeZr/T catalysts. Based on the characterization of the catalyst structures and catalytic behaviors, the support effects of TiO_2 or ZSM-5 on CO catalytic ignition were investigated by *in situ* infrared coupled with a magnetically driven cell. The conclusions reached from these results are as follows:

(1) The ignition profiles obtained for the CuCeZr/Z, CuCeZr/T and CuCeZr catalysts show similar structures but with different ignition temperatures of 175 °C, 146 °C and 63 °C, respectively, under a feed gas of 10 vol.% CO + 10 vol.% O_2 + 80 vol.% N_2, and corresponding stability limits, as reflected by the Φ values at a flow rate of 200 mL/min with values of 0.122, 0.114 and 0.052, respectively. The CuCeZr catalyst exhibited excellent stability for self-sustained CO combustion, as evaluated by a 100-h time-on-stream study. However, deactivation occurred for the CuCeZr/Z catalyst after maintaining the combustion process for only 27.4 h due to the production of coke on the Brønsted acid sites.

(2) The Cu^+ cations located at the gas-solid phase interface are the main active sites. As a rate-determining step for self-sustained CO combustion, CO adsorption and activation mainly take place at these sites. The interactions of Cu and Ce lead to the formation of Cu-Ce solid solutions in CuCeZr. With respect to CuCeZr/T and CuCeZr/Z, however, CO oxidation mainly occurs at the phase interface between the copper oxides and TiO_2/ZSM-5. The TiO_2 and ZSM-5 supports promote the dispersion of copper species, particularly for TiO_2, while the Cu-Ce interactions seem to be less relevant. A well copper dispersion results in a redshift of the carbonyl bands and an increase in CO adsorption onto CuCeZr/T and CuCeZr/Z, which are believed to enhance the activities of individual copper sites. Close interactions between Cu and Ce with high surface contents are conducive to the local accumulation of heat and mass transfer over bulk CuCeZr, leading to the ignition of CO at low temperatures.

(3) The reaction pathways are proposed as follows. The activities of the catalysts

toward CO combustion are mainly determined by the Cu^{+} cations, which are the main active sites, and superficially active oxygen. With respect to CuCeZr, CO is first adsorbed onto the oxygen vacancies at the interface between the Cu and Ce oxides to form [Cu^{+}-(C≡O)-Ce^{3+}] at low temperatures. In addition to the inactive carbonates, the monocarbonyls [Cu^{+}-CO], which are more likely to replace [Cu^{+}-(C≡O)-Ce^{3+}] at high temperatures, are the dominant active species for CO oxidation, and the vacancies occupied by oxygen accelerate the oxygen cycles. For CuCeZr/T and CuCeZr/Z, however, the dicarbonyls [$Cu^{+}(CO)_2$] are mainly replaced by the monocarbonyls [Cu^{+}-CO] at high temperatures as the main intermediates for CO oxidation, and the agglomerated Cu^{2+} species are reduced by the oxygen attached to the copper sites, which also takes part in the oxidation process.

Declaration of Competing Interest

The authors declare that they have no known competing financial interests or personal relationships that could have appeared to influence the work reported in this paper.

CRediT authorship contribution statement

Running Kang: Conceptualization, Methodology, Data curation, Formal analysis, Investigation, Visualization, Writing-original draft, Writing-review & editing. **Zirui Zhang**: Data curation, Formal analysis. **Feng Bin**: Conceptualization, Supervision, Funding acquisition, Project administration, Writing-review & editing.

Xiaolin Wei: Resources, Project administration, Investigation. **Yongdan Li**: Supervision, Writing-review & editing. **Guoxing Chen**: Supervision, Formal analysis, Writing-review & editing. **Xin Tu**: Conceptualization, Supervision, Writing-review & editing.

Acknowledgments

We gratefully acknowledge the financial support from the National Natural Science Foundation of China (No. 52176141) and the Strategic Priority Research Program of the Chinese Academy of Sciences (No. XDA21040500). R. Kang acknowledges the support from the China Scholarship Council (No. 202004910623).

References

[1] N. Ma. Recycling of basic oxygen furnace steelmaking dust by in-process separation of zinc from the dust. J. Cleaner Production. 112 (2016) 4497–4504.

[2] S. Li, X. Wei, L. Yu. Numerical simulation of off-gas formation during top-blown oxygen converter steelmaking. Fuel. 90 (2011) 1350–1360.

[3] F. Bin, X. Wei, B. Li. Self-sustained combustion of carbon monoxide promoted by the Cu-Ce/ZSM-5 catalyst in $CO/O_2/N_2$ atmosphere. Appl. Catal. B: Environ. 162 (2015) 282–288.

[4] S. Tacchino, L. D. Vella, S. Specchia. Catalytic combustion of CH_4 and H_2 into micro-monoliths. Catal. Today. 157 (2010) 440–445.

[5] E. Newson, T. B. Truong. Low-temperature catalytic partial oxidation of hydrocarbons (C_1–C_{10}) for hydrogen production. Int. J. Hydrogen Energ. 28 (2003) 1379–1386.

[6] R.N. Kang, X.L. Wei, P.D. Ma, F. Bin, J.Y. He, Q.L. Hao, B.J. Dou. Self-sustained combustion of CO with transient changes and reaction mechanism over

$CuCe_{0.75}Zr_{0.25}O_{\delta}$ powder for honeycomb ceramic catalyst. Fuel. 263 (2020), 116637.

[7] F. Bin, R.N. Kang, X.L. Wei, Q.L. Hao, B.J. Dou. Self-sustained combustion of carbon monoxide over $CuCe_{0.75}Zr_{0.25}O_{\delta}$ catalyst: Stability operation and reaction mechanism. Proc. Combust. Inst. 37(4) (2019) 5507–5515.

[8] R.N. Kang, P.D. Ma, J.Y. He, H.X. Li, F. Bin, X.L. Wei, B.J. Dou, K.N. Hui, K.S. Hui. Transient behavior and reaction mechanism of CO catalytic ignition over a $CuO–CeO_2$ mixed oxide. Proc. Combust. Inst. 38 (2021) 6493–6501.

[9] P. S. Barbato, G. Landi, R. Pirone, G. Russo, A. Scarpa, Auto-thermal combustion of CH_4 and CH_4-H_2 mixtures over bi-functional Pt-$LaMnO_3$ catalytic honeycomb. Catal. Today. 147S (2009) S271-S278.

[10] J. Lu, J. Wang, Q. Zou, D. He, L. Zhang, Z. Xu, S. He, Y. Luo. Unravelling the nature of the active species as well as the doping effect over Cu/Ce-based catalyst for carbon monoxide preferential oxidation. J. Catal. 9 (2019) 2177–2195.

[11] H. He, H.X. Dai, K.W. Wong, C.T. Au, $RE_{0.6}Zr_{0.4-x}Y_xO_2$ (RE = Ce, Pr; x = 0, 0.05) solid solutions: an investigation on defective structure, oxygen mobility, oxygen storage capacity, and redox properties. Appl. Catal. A: Gen. 251 (2003) 61–74.

[12] R. D. Zhang, W. Y. Teoh, R. Amal, B. H. Chen, S. Kaliaguine, Catalytic reduction of NO by CO over $Cu/Ce_xZr_{1-x}O_2$ prepared by flame synthesis. J. Catal. 272 (2010) 210–219.

[13] Y.N. Zheng, K.Z. Li, H. Wang, Y.H. Wang, D.Tian, Y.G. Wei, X. Zhu, C.H. Zeng, Y.M. Luo, Structure dependence and reaction mechanism of CO oxidation: A model study on macroporous CeO_2 and CeO_2-ZrO_2 catalysts. J. Catal. 344 (2016) 365–377.

[14] A.P. Jia, G.S. Hu, L. Meng, Y.L. Xie, J.Q. Lu, M.F. Luo, CO oxidation over $CuO/Ce_{1-x}Cu_xO_{2-\delta}$ and $Ce_{1-x}Cu_xO_{2-\delta}$ catalysts: Synergetic effects and kinetic study. J. Catal. 289 (2012) 199–209.

[15] M. S. P. Francisco, V. R. Mastelaro, Activity and characterization by XPS, HR-TEM, Raman spectroscopy, and BET surface area of CuO/CeO_2-TiO_2 catalysts. J. Phys. Chem. B. 105 (2001) 10515–10522.

[16] S. Li, Q. Hao, R. Zhao, D. Liu, H. Duan, B. Dou, Highly efficient catalytic removal of ethyl acetate over Ce/Zr promoted copper/ZSM-5 catalysts. Chem. Eng. J. 285 (2016) 536–543.

[17] I. X. Green, W. Tang, M. Neurock, J. T. Yates Jr., Spectroscopic observation of dual catalytic sites during oxidation of CO on a Au/TiO_2 catalyst. Science. 333 (2011) 736–739.

[18] D. Vogel, C. Spiel, Y. Suchorski, A. Trinchero, R. Schlçgl, H. Grçnbeck, G. Rupprechter, Local catalytic ignition during CO oxidation on low-index Pt and Pd surfaces: A combined PEEM, MS, and DFT study. Angew. Chem. Int. Ed. 51 (2012) 10041–10044.

[19] S. D. Senanayake, N. A. Pappoe, T. Nguyen-phan, Interfacial Cu^+ promoted surface reactivity: Carbon monoxide oxidation reaction over polycrystalline copper-titania catalysts. Surf. Sci. 652 (2016) 206–212.

[20] R.Z. Zhao, Q.L. Hao, F. Bin, R.N. Kang, B.J. Dou, Influence of Ce/Zr ratio on the synergistic effect over $CuCe_{1-x}Zr_xO_y$/ZSM-5 catalysts for the self-sustained combustion of carbon monoxide. Combust. Sci. Tech. 189 (2017) 1394–1415.

[21] Z. Y. Pu, X. S. Liu, A. P. Jia, Y. L. Xie, J. Q. Lu, M. F. Luo, Enhanced activity for CO oxidation over Pr-and Cu-doped CeO_2 catalysts: effect of oxygen vacancies. J. Phys. Chem. C. 112 (2008) 15045–15051.

[22] J. Deng, Z.M. Luo, X.C. Wu, Y.Y. Hu. Explosive limits of mixed gases containing CH_4, CO and C_2H_4 in the goaf area. Mining Sci. Tech. 20 (2010) 0557–0562.

[23] F. Bin, C. Song, G. Lv, J. Song, S. Wu, X. Li. Selective catalytic reduction of nitric oxide with ammonia over zirconium-doped copper/ZSM-5 catalysts. Appl. Catal. B: Environ. 150-151 (2014) 532–543.

[24] H. Yoshida, N. Yamashita, S. Ijichi, Y. Okabe, S. Misumi, S. Hinokuma, M. Machida. A thermally stable Cr–Cu nanostructure embedded in the CeO_2 surface as a substitute for platinum-group metal catalysts. ACS Catal. 5 (2015) 6738–6747.

[25] A.P. Jia, S.Y. Jiang, J.Q. Lu, M.F. Luo, Study of catalytic activity at the

CuO-CeO_2 interface for CO oxidation. J. Phys. Chem. C. 114 (2010) 21605–21610.

[26] T. Tsoncheva, G. Issa, T. Blasco, P. Concepcion, M. Dimitrov, S. Hernández, D. Kovacheva, G. Atanasova, J. M. López Nieto. Silica supported copper and cerium oxide catalysts for ethyl acetate oxidation. J. Colloid. Interf. Sci. 404 (2013) 155–160.

[27] G.X. Chen, Q.L. Li, Y.C. Wei, W.P. Fang, Y.Q. Yang. Low temperature CO oxidation on Ni-promoted CuO-CeO_2 catalysts. Chinese J. Catal. 34 (2013) 322–329.

[28] H. Ha, S. Yoon, K. An, H.Y. Kim. Catalytic CO oxidation over Au nanoparticles supported on CeO_2 nanocrystals: effect of the Au–CeO_2 interface. ACS Catal. 11 (2021) 1516–1527.

[29] Q. Wan, L. Duan, K. He, J. Li. Removal of gaseous elemental mercury over a CeO_2–WO_3/TiO_2 nanocomposite in simulated coal-fired flue gas. Chem. Eng. J. 170 (2011) 512–517.

[30] F. Li, B. Cao, R. Ma, J. Liang, H. Song. H. Song. Performance of Cu/TiO_2-SiO_2 catalysts in Hydrogenation of furfural to furfuryl alcohol. Can. J. Chem. Eng. 94 (2016) 1368–1374.

[31] S. Karnjanakom, A. Yoshida, A. Bayu, I. Kurnia, X. Hao, P. Maneechakr, A. Abudula, G. Guan. Bifunctional Mg-Cu-Loaded b-Zeolite: High Selectivity for the Conversion of Furfural into Monoaromatic Compounds. ChemCatChem. 10 (2018) 3564–3575.

[32] A. A. Ibrahim, A. A. Al-Fatesh. H. Atia, A. H. Fakeeha, S. O. Kasim, A. E. Abasaeed. Influence of promoted 5%Ni/MCM-41 catalysts on hydrogen yield in CO_2 reforming of CH_4. Int. J. Energy Res. 42 (2018) 4120–4130.

[33] P. A. Carlsson, M. Skoglundh. Low-temperature oxidation of carbon monoxide and methane over alumina and ceria supported platinum catalysts. Appl. Catal. B: Environ. 101 (2011) 669–675.

[34] E. E. Iojoiu, B. Bassou, N. Guihaume, D. Farrusseng, A. Desmartin-Chomel, K. Lombaert, D. Bianchi, C. Mirodatos. High-throughput approach to the catalytic

combustion of diesel soot. Catal. Today. 137 (2008) 103–109.

[35] A. Penkova, L. F. Bobadilla, F. Romero-Sarri, M. A. Centeno, J. A. Odriozola. Pyridine adsorption on NiSn/MgO-Al_2O_3: An FTIR spectroscopic study of surface acidity. Appl. Sur. Sci. 317 (2014) 241–251.

[36] F. F. Madeira, K. B. Tayeb, L. Pinard, H. Vezin, S. Maury, N. Cadran. Ethanol transformation into hydrocarbons on ZSM-5 zeolites: Influence of Si/Al ratio on catalytic performances and deactivation rate. Study of the radical species role. Appl. Catal. A: Gen. 443–444 (2012) 171–180.

[37] J. P. Holman. Heat Transfer, The McGraw-Hill Companies, Inc, 2010.

[38] A.P. Nunez, I. Jbir, D. Bianchi, F.C. Meunier. Spectrum baseline artefacts and correction of gas-phase species signal during diffuse reflectance FT-IR analyses of catalysts at variable temperatures. Appl. Catal. A: Gen. 495 (2015) 17–22.

[39] R.N. Kang, J.Q. Huang, F. Bin, Z.H. Teng, X.L. Wei, B.J. Dou, S. Kasipandi. Evolution behavior and active oxygen quantification of reaction mechanism on cube Cu_2O for CO self-sustained catalytic combustion and chemical-looping combustion. Appl. Catal. B Environ, 310 (2022), 121296.

[40] P. Xie, Z. Ma, H.B. Zhou. C.Y. Huang, Y.H. Yue. W. Shen, H.L. Xu, W.M. Hua, Z. Gao. Catalytic decomposition of N_2O over Cu-ZSM-11 catalysts. Micropor. Mesopor. Mat. 191 (2014) 112–117.

[41] A. Hornés, P. Bera, A. L. Cámara, D. Gamrra, G. Munuera, A. Martínez-Arias. CO-TPR-DRIFT-MS in situ of $CuO/Ce_{1-x}Tb_xO_{2-y}$ (x=0, 0.2, and 0.5) catalysts: Support effects on redox properties and CO oxidation catalysts, J. Catal. 268 (2009) 367–375.

[42] R.N. Kang, X.L. Wei, F. Bin, Z.B. Wang, Q.L. Hao, B.J. Dou. Reaction mechanism and kinetics of CO oxidation over a $CuO/Ce_{0.75}Zr_{0.25}O_{2-\delta}$ catalyst. Appl. Catal. A, Gen. 565 (2018) 46–58.

[43] Y. Wang, D. Widmann, F. Lehnert, D. Gu, F. Schgth, R. Jgrgen Behm. Avoiding self-poisoning: a key feature for the high activity of $Au/Mg(OH)_2$ catalysts in continuous low-temperature CO oxidation. Angew. Chem. Int. Ed. 56 (2017) 9597–9602.

[44] P. Bera, A. L. Cámara, A. Hornés, A. Martínez-Arias. Comparative in situ DRIFT-MS study of ^{12}CO and ^{13}CO-TPR on CuO/CeO_2 catalyst. J. Phys. Chem. C 113 (2009) 10689–10695.

[45] M. J. Pollard, B. A. Weinstock, T. E. Bitterwolf, P. R. Griffiths, A. P. Newbery, J. B. Paine. A mechanistic study of the low-temperature conversion of carbon monoxide to carbon dioxide over a cobalt oxide catalyst. J. Catal 254 (2008) 218–225.

[46] K. I. Hadjiivanov, M. M. Kantcheva, D. G. Klissurski. IR study of CO adsorption on Cu-ZSM-5 and CuO/SiO_2 catalysts: σ and π components of the Cu^+-CO bond, J. Chem. Soc. Faraday Trans. 92 (1996) 4595–4600.

[47] T. T. H. Dang, H. Zubowa, U. Bentrup, M. Richter, A. Martin. Microwave-assisted synthesis and characterization of Cu-containing $AlPO_4$-5 and SAPO-5. Micropor. Mesopor. Mat. 123 (2009) 209–220.

[48] J. Y. Yan, G. D. Lei, W. M. H. Sachtler, H. H. Kung. Deactivation of Cu/ZSM-5 catalysts for lean NO_x reduction: characterization of changes of Cu state and zeolite support. J. Catal. 161 (1996) 43–54.

[49] Z.H. Zhang, L.P. Fan, W.Q. Liao, F.Y. Zhao, C. Tang, J. Zhang, M. Feng, J.Q. Lu. Structure sensitivity of CuO in CO oxidation over CeO_2-CuO/Cu_2O catalysts. J. Catal. 405 (2022) 333–345.

[50] P.D. Ma, C.H. Zhang, B.J. Dou, X.K. Yi, F. Bin, W.J. Liang. Synthesis of Cu2O micro/nanocrystals for catalytic combustion of high-concentration CO: The crucial role of glucose. Chemosphere. 314 (2023) 137720.

[51] R. Si, J. Liu, K. Yang, X. Chen, W. Dai, X. Fu. Temperature-programed surface reaction study of CO oxidation over Au/TiO_2 at low temperature: An insight into nature of the reaction process. J. Catal. 311 (2014) 71–79.